

Strong Second Harmonic Generation from the Tantalum Thioarsenates $A_3Ta_2AsS_{11}$ ($A = K$ and Rb)

Tarun K. Bera,[†] Joon I. Jang,[‡] John B. Ketterson,[‡] and Mercuri G. Kanatzidis^{*,†,§}

Department of Chemistry, Northwestern University, Evanston, Illinois 60208, Department of Physics and Astronomy, Northwestern University, Evanston, Illinois 60208, and Materials Science Division, Argonne National Laboratory, Argonne, Illinois 60439

Received October 13, 2008; E-mail: m-kanatzidis@northwestern.edu

Noncentrosymmetric (NCS) semiconductors can exhibit second harmonic generation (SHG) nonlinear optical (NLO) response in the mid-IR (2–20 μm) region, a spectral range of importance for molecular spectroscopy, atmospheric sensing, communications and various optoelectronic devices.¹ The use of oxides, e.g., KTiOPO₄ (KTP), LiB₃O₅ (LBO), β -BaB₂O₄ (BBO), LiNbO₃ (LN), etc., which are the benchmark materials in the UV–vis to near-infrared (IR) region of the spectrum, is limited in the mid-IR region because of inadequate optical transparency and relatively low SHG efficiency.² Chalcogenide semiconductors are more promising in the IR,³ but only a few, for example, AgGaSe₂, AgGaS₂, GaSe, possess the necessary SHG susceptibility, optical transparency, chemical stability, etc. for technological applications.⁴ Recent studies in search for new NCS oxides with high SHG susceptibility are aimed at introducing asymmetric building units, such as second-order Jahn–Teller (SOJT) distorted d^0 metal centers (e.g., Ti⁴⁺, Ta⁵⁺, Mo⁶⁺, etc.),⁵ anionic groups with stereochemically active lone pairs [e.g., (IO₃)¹⁻, (TeO₃)ⁿ⁻, etc.],⁶ and noncentrosymmetric π -orbital systems [e.g., (BO₃)³⁻ and (B₃O₆)³⁻].⁷ Corresponding units in the chalcogenides, (e.g., polar [AsS₃]³⁻, [SbS₃]³⁻, [TeS₃]²⁻, etc.)⁸ have been little explored in the context of NLO properties.

Our recent investigation of the $A/\text{As}/\text{S}$ ($A = \text{Li}$ and Na) system revealed the soluble polar direct-band gap material Li_{1-x}Na_xAsS₂ (contains pyramidal [AsS₃]³⁻ units) with high SHG efficiency, which can approach ~ 30 times relative to the benchmark IR material AgGaSe₂.⁹ Improvements of the SHG efficiency by introducing multiple asymmetric building units into the structure have been reported, e.g., both SOJT distorted d^0 metal centers and anionic groups with stereochemically active lone pairs in BaTeMo₂O₉, TiTeVO₅, etc.¹⁰ SOJT distorted d^0 metal cations in oxides are abundant, whereas in the chalcogenide structures are less common owing to weaker M–S interactions relative to those of M–O. CsTaS₃ is an example of d^0 metal chalcogenide, where the Ta⁵⁺ displacement from SOJT effect.¹¹ Our investigation in the $A/\text{Ta}/\text{As}/\text{S}$ ($A = \text{monovalent cations}$) system was motivated by the idea of introducing two different asymmetric units; [Ta_mS_n]^{p-} and [AsS₃]³⁻ in a single NCS structure. Here we report the synthesis and properties of K₃Ta₂AsS₁₁ (**Ia**), Rb₃Ta₂AsS₁₁ (**Ib**), and Cs₃Ta₂AsS₁₁ (**II**). We find that the NLO SHG of crystals of **Ia–b** is up to ~ 15 times stronger than that of commercially used AgGaSe₂.

Phase pure syntheses of **Ia**, **Ib**, and **II** were achieved¹² with the alkali-metal polythioarsenate flux method using A₂S/Ta/As/S mixtures.¹³ The purity of materials was confirmed by comparing powder X-ray diffraction patterns with those simulated from the single crystal X-ray diffraction analysis. The flux basicity (i.e., determined by the A₂S/S ratio) plays a crucial role in the synthesis of pure phase. The relatively basic flux ratios of 1/1/1/4 or 3/1/1/12 did not produce the title phase; instead gave compounds without arsenic namely black

ATaS₃¹¹ and orange A₄Ta₂S₁₁.¹⁴ A decrease of the flux basicity, which was achieved by increasing the relative S fraction, led to appreciable proportions of the title quaternary compound and finally 1/1/1/12 was found to be the optimum flux ratio to produce pure A₃Ta₂AsS₁₁. The air and moisture stable orange-red compounds were further characterized with electronic absorption spectroscopy, Raman spectroscopy and differential thermal analysis (see below). A medium size crystal of **Ib** (1.0 \times 0.45 \times 0.24 mm³) isolated from the flux reaction is shown in Figure 1a.

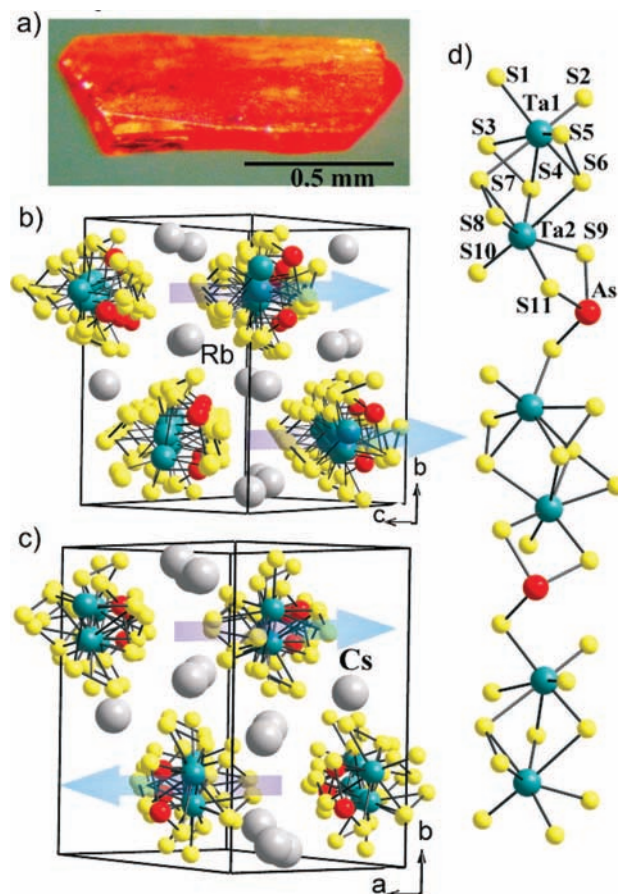


Figure 1. (a) Photo of a medium-size crystal of Rb₃Ta₂AsS₁₁ grown in a polysulfide flux. (b) Noncentrosymmetric packing of the $1/\infty[\text{Ta}_2\text{AsS}_{11}^{3-}]$ chains in **Ia–b**. The in-phase arrangement of chains is shown by the pale blue arrows. (c) Centrosymmetric packing of the $1/\infty[\text{Ta}_2\text{AsS}_{11}^{3-}]$ chain in **II**. (d) A single $1/\infty[\text{Ta}_2\text{AsS}_{11}^{3-}]$ chain, showing the connectivity between AsS₃ trigonal pyramids and asymmetric [Ta₂S₁₁]⁶⁻ units.

Compounds **Ia** and **Ib** crystallize¹⁵ in the monoclinic space group *Cc* whereas **II** crystallizes in *P2₁/n*. All compounds contain the same

[†] Department of Chemistry, Northwestern University.

[‡] Department of Physics and Astronomy, Northwestern University.

[§] Argonne National Laboratory.

parallel $1/\infty[\text{Ta}_2\text{AsS}_{11}^{3-}]$ polymeric anionic chains, (Figure 1b, 1c). The size of the alkali-metals has a profound effect on the packing of the chains. The K^+ or Rb^+ favor noncentrosymmetric packing (Figure 1b) of the $1/\infty[\text{Ta}_2\text{AsS}_{11}^{3-}]$ chains, whereas the larger Cs^+ favors the centrosymmetric packing (Figure 1c). The cross-section of a chain is irregular and the noncentrosymmetric packing arises from the in-phase alignment of the AsS_3 pyramids. The structure of the $1/\infty[\text{Ta}_2\text{AsS}_{11}^{3-}]$ chain is similar to its Se analogue.¹⁶ The chain is a polysulfide species, which is build up of bimetallic $[\text{Ta}_2\text{S}_{11}]^{6-}$ units linked with AsS_3 pyramids (Figure 1d).

Conceptually, the chain derives from the oxidative insertion of As into the S–S units of the $[\text{Ta}_4\text{S}_{22}]^{6-}$ core¹⁷ as shown in eq 1. The common dimeric core $[\text{Ta}_2\text{S}_{11}]^{6-}$,¹⁴ derives from the trigonal face sharing of two distorted TaS_7 pentagonal bipyramids. It can be best described as $[\text{Ta}_2\text{S}_5(\text{S}_2)_3]^{6-}$, where the S–S distances [2.063(2)–2.098(2) Å] are within the range of typical S_2^{2-} anion.¹⁸



The presence of disulfide (S_2)²⁻ units in TaS_7 was confirmed by the intense peaks in the range 485–525 cm^{-1} in the Raman spectrum (Figure 2a).¹⁸ All As–S bond distances are normal¹⁹ and A–S (A = K, Rb, and Cs) bonds are mostly ionic in nature.

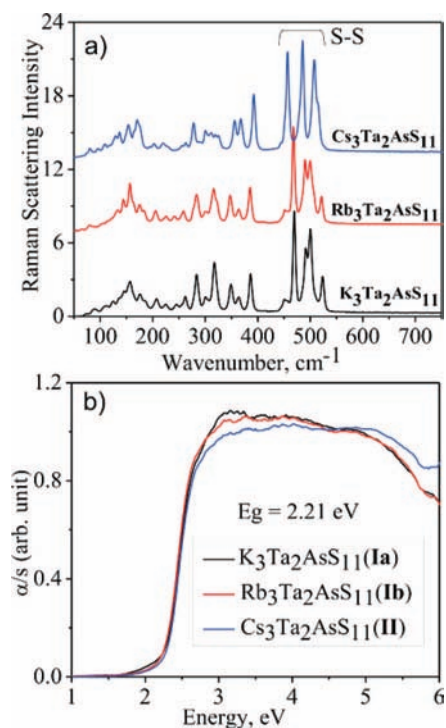


Figure 2. (a) Raman spectra of **Ia**, **Ib**, and **II**, showing the characteristic shift from disulfide anion (S_2)²⁻. (b) Solid-state UV–vis optical absorption spectrum of **Ia**, **Ib**, and **II**, shows sharp absorption edge at 2.21 eV.

Electronic absorption spectroscopy of the solid samples showed a sharp absorption edge at 2.21 eV for all three compounds consistent with their orange color (Figure 2b). The alkali-metal ions have negligible effect on the energy gap suggesting purely ionic interactions with the $1/\infty[\text{Ta}_2\text{AsS}_{11}^{3-}]$ chains. The optical excitation is believed to originate from S-based *p*-orbital dominating valance band to the Ta-based orbitals in the conduction band.²⁰

Differential thermal analysis (DTA) confirmed that all three compounds melt incongruently (see the Supporting Information). Both melting and crystallization points are within 400–500 °C for all three compounds and those values decrease on going from **Ia** (K) to **Ib** (Rb)

to **II** (Cs). Though single melting and crystallization peaks were observed in the DTA plots, powder X-ray diffraction done after DTA, showed extra diffraction peaks along with the title compounds, suggesting thermal decomposition. For **Ib**, the black decomposition product observed after DTA was identified as RbTaS_3 ,²¹ whereas that for **II** was CsTaS_3 .¹¹ Since the syntheses of the compounds were achieved at 550 °C, which is above their melting points, it is apparent that the polysulfide flux allows for the formation of the incongruently melting phases in pure crystalline form either during the soaking time or on cooling. Thus, large optical quality crystals could best be obtained by the flux technique as in the case of $\text{A}_2\text{Hg}_3\text{M}_2\text{S}_8$ (A = K, Rb; M = Ge, Sn).²²

The excellent nonlinear optical SHG response is the most significant property of the polar compounds **Ia** and **Ib**. It was measured with a variable wavelength (1000–2000 nm) laser source using a modified Kurtz and Perry method (see the Supporting Information).²³ A comparison of the SHG response relative to the benchmark material AgGaSe_2 was also done using the same particle size ranges mainly in the wavelength > 700 nm, Figure 3. Efficiency comparison below 700

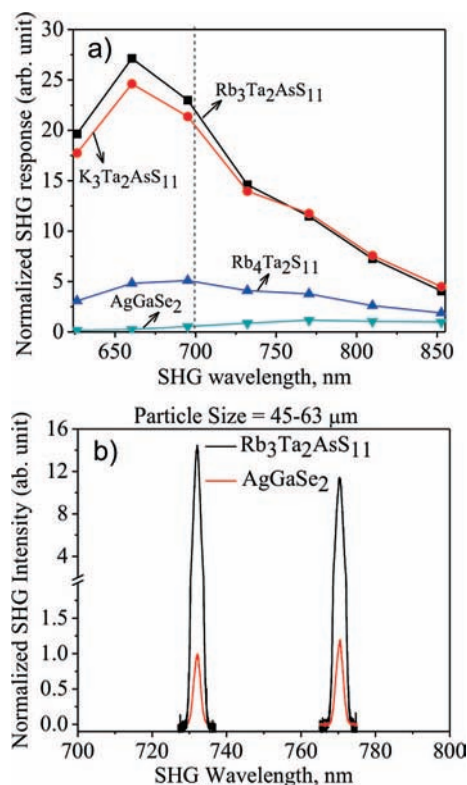


Figure 3. (a) Comparison of the SHG response of **Ia**, **Ib**, and $\text{Rb}_4\text{Ta}_2\text{S}_{11}$, relative to AgGaSe_2 at different SHG wavelength, using powder samples (average particle size of $54 (\pm 9) \mu\text{m}$). The solid lines between the points are a guide to the eye. The vertical dotted line represents the band-edge (1.80 eV) of AgGaSe_2 . (b) Overlay of SHG signals from $\text{Rb}_3\text{Ta}_2\text{AsS}_{11}$ and AgGaSe_2 at two different wavelengths. In both cases the average particle size was $54 (\pm 9) \mu\text{m}$.

nm is not reliable because of the band-edge absorption of AgGaSe_2 . In the range 700–900 nm the SHG efficiency was ~15 times stronger than that of AgGaSe_2 and comparable to the recently reported CsZrPSe_6 .²⁴ Particle size dependent SHG measurements indicated that both **Ia** and **Ib** are type-I nonphase-matchable at 770 nm. Generally, when a powder sample is nonphase-matchable, SHG sensitivity peaks near the coherence length, which is typically 1–20 μm , and it start to diminish through larger particle sizes. Despite this such materials can still be used through ‘random’ quasi-phase-matching techniques.²⁵

phase-matchability also varies with wavelength, for example AgGaSe₂ is phase-matchable only in the range of 3800–12400 nm.²⁶ So, it is possible that **Ia–b** are phase-matchable at a different wavelength range beyond the one studied here. The highly polar structure that results from the alignment of dipoles in **Ia–b** (cf. Figure 1b) is likely responsible for the enhanced SHG intensity compared to AgGaSe₂, which is only weakly polar. Unlike the Li_{1-x}Na_xAsS₂ system, where we observed a systematic increase of the SHG efficiency with *x*,⁹ the efficiency of both end-members (**Ia** and **Ib**) of K_{3-x}Rb_xTa₂AsS₁₁ system are similar (cf. Figure 3), suggesting negligible contribution from the alkali-metal polarizability.

To better assess the relative contribution of the pyramidal [AsS₃]³⁻ and [Ta₂S₁₁]⁶⁻ units toward the total polarizability, we examined the NLO properties of Rb₄Ta₂S₁₁, a related NCS compound with similar chains containing the polysulfide unit of [Ta₂S₁₁]⁴⁻ but no [AsS₃]³⁻ units.¹⁴ The SHG response of Rb₄Ta₂S₁₁ was found to be strong but only ~4× that of AgGaSe₂, Figure 3. This result is suggestive of the predominant role of the pyramidal [AsS₃]³⁻ unit on the total polarity and consequently on the SHG response of the **Ib**.

In conclusion, the polysulfide flux is critical in stabilizing the strongly anisotropic thioarsenates A₃Ta₂AsS₁₁. The combination of two asymmetric units, [Ta₂S₁₁] and [AsS₃], in a single strand coupled with polar packing of strands appears to lead to strong NLO SHG response. This implies that the approach of combing different asymmetric fragments (e.g., chalcogenides) to impart strong polarity in extended structures could be promising in finding exceptional candidate materials for NLO applications. The results of this study also justify future synthetic investigations in the A/M/As/Q systems (A = monovalent cations; M = V, Nb, Ta; Q = S, Se, Te).

Acknowledgment. Financial support from the National Science Foundation (Grant DMR-0801855) is gratefully acknowledged. This work made use of the SEM facilities at the Electron Probe Instrumentation Center (EPIC), Northwestern University. FT-Raman spectroscopic study was done at the Analytical Service Laboratory (ASL), Northwestern University.

Supporting Information Available: X-ray crystallographic files (CIF) and experimental details for K₃Ta₂AsS₁₁, Rb₃Ta₂AsS₁₁, and Cs₃Ta₂AsS₁₁. This material is available free of charge via the Internet at <http://pubs.acs.org>.

References

- (1) (a) Ebrahim-Zadeh, M.; Sorokina, I. T. *Mid-Infrared Coherent Sources and Applications*; NATO Science for Peace and Security Series B: Physics and Biophysics; Springer: New York, 2007. (b) Nikogosyan, D. N. *Nonlinear optical crystals: a complete survey*; Springer-Science: New York, 2005. (c) Goodman, C. H. L. *Semicond. Sci. Technol.* **1991**, *6*, 725.
- (2) Fossier, S.; et al. *J. Opt. Soc. Am. B* **2004**, *21*, 1981.
- (3) (a) Schunemann, P. G. *Proc. SPIE* **2007**, *6455*, 64550R-1. (b) Petrov, V. B.; Panyutin, V. V. *Quaternary Nonlinear Optical Crystals for the Mid-Infrared Spectral Range from 5 to 12 μm*; NATO Science for Peace and Security Series B: Physics and Biophysics; Springer: New York, 2007; pp 105–147.
- (4) Bordui, P. F.; Fejer, M. M. *Annu. Rev. Mat. Sci.* **1993**, *23*, 321.
- (5) (a) Halasyamani, P. S. *Chem. Mater.* **2004**, *16*, 3586. (b) Muller, E. A.; Cannon, R. J.; Sarjeant, A. N.; Ok, K. M.; Halasyamani, P. S.; Norquist, A. J. *Cryst. Growth Des.* **2005**, *5*, 1913.
- (6) (a) Chi, E. O.; Ok, K. M.; Porter, Y.; Halasyamani, P. S. *Chem. Mater.* **2006**, *18*, 2070. (b) Phanon, D.; Gautier-Luneau, I. *Angew. Chem., Int. Ed.* **2007**, *46*, 8488.
- (7) (a) Pan, S.; Smit, J. P.; Watkins, B.; Marvel, M. R.; Stern, C. L.; Poeppelmeier, K. R. *J. Am. Chem. Soc.* **2006**, *128*, 11631. (b) Sasaki, T.; Mori, Y.; Yoshimura, M.; Yap, Y. K.; Kamimura, T. *Mater. Sci. Eng., R* **2000**, *30*, 1. (c) Chen, C.; Lin, Z.; Wang, Z. *Appl. Phys. B: Laser Opt.* **2005**, *80* (1), 1–25.
- (8) (a) Ye, N.; Chen, Q.; Wu, B.; Chen, C. *J. Appl. Phys.* **1998**, *84*, 555. (b) Distanov, V. E.; Nenashev, B. G.; Kiryashkin, A. G.; Serboulenko, M. G. *Proustite J. Crystal Growth* **2002**, *235*, 457. (c) Feichtner, J. D.; Roland, G. W. *J. Appl. Opt.* **1972**, *11*, 993. (d) Zhang, X.; Kanatzidis, M. G. *J. Am. Chem. Soc.* **1994**, *116*, 1890. (e) McCarthy, T. J.; Kanatzidis, M. G. *Chem. Mater.* **1993**, *5*, 1061. (f) Chondroudis, K.; McCarthy, T. J.; Kanatzidis, M. G. *Inorg. Chem.* **1996**, *35*, 840.
- (9) Bera, T. K.; Song, J. H.; Freeman, A. J.; Jang, J. I.; Ketterson, J. B.; Kanatzidis, M. G. *Angew. Chem., Int. Ed.* **2008**, *120*, 7946.
- (10) (a) Sivakumar, T.; Chang, H. Y.; Baek, J.; Halasyamani, P. S. *Chem. Mater.* **2007**, *19*, 4710. (b) Ra, H. S.; Ok, K. M.; Halasyamani, P. S. *J. Am. Chem. Soc.* **2003**, *125*, 7764.
- (11) Pell, M. A.; Vajenine, G. V. M.; Ibers, J. A. *J. Am. Chem. Soc.* **1997**, *119*, 5186.
- (12) K₃Ta₂AsS₁₁(**Ia**). A mixture of K₂S (0.050 g, 0.45 mmol), Ta (0.082 g, 0.45 mmol), As (0.034 g, 0.45 mmol), and S (0.175 g, 5.45 mmol) was loaded into a fused-silica tube in a nitrogen-filled glovebox. It was flame-sealed under vacuum (~10⁻⁴ mbar) and then heated to 550 °C in 6 h. After 48 h of soaking it was cooled down to 250 °C in 60 h followed by rapid cooling to room temperature. An orange-red color compound was isolated as a single phase in >60% yield after dissolution of the excess flux with degassed DMF and unreacted sulfur with CS₂. Semiquantitative energy dispersive analysis (EDS) gave an average composition of K_{3.1}Ta_{2.2}As_{1.2}S_{12.1}; Rb₃Ta₂AsS₁₁(**Ib**). A mixture of Rb₂S (0.081 g, 0.40 mmol), Ta (0.052 g, 0.40 mmol), As (0.030 g, 0.40 mmol), and S (0.154 g, 4.80 mmol) was loaded into a fused-silica tube in a nitrogen-filled glovebox. It was flame-sealed under vacuum (~10⁻⁴ mbar) and then application of a heating and cooling cycle similar to that above, produced orange-red crystalline product as a single phase in >65% yield. Semiquantitative energy dispersive analysis (EDS) gave an average composition of Rb_{3.3}Ta_{2.1}As_{1.2}S_{11.8}; Cs₃Ta₂AsS₁₁(**II**). It was isolated from the reaction of Cs₂S (0.107 g, 0.36 mmol), Ta (0.065 g, 0.36 mmol), As (0.027 g, 0.36 mmol), and S (0.139 g, 4.32 mmol) using a procedure similar to that above. The compound was obtained as a single phase in >60% yield after dissolving the excess flux with degassed DMF and unreacted sulfur with CS₂. EDS analysis gave an average composition of Cs_{3.2}Ta_{2.1}As_{1.1}S_{11.9}.
- (13) (a) Sunshine, S. A.; Kang, D.; Ibers, J. A. *J. Am. Chem. Soc.* **1987**, *109*, 6202. (b) Kanatzidis, M. G.; Sutorik, A. C. *Prog. Inorg. Chem.* **1995**, *43*, 151. (c) Bera, T. K.; Iyer, R. G.; Malliakas, C. D.; Kanatzidis, M. G. *Inorg. Chem.* **2007**, *46*, 8466. (d) Bera, T. K.; Kanatzidis, M. G. *Inorg. Chem.* **2008**, *47*, 7068.
- (14) Durichen, P.; Bensch, W. *Acta Crystallogr., Sect. C* **1998**, *54*, 706.
- (15) Single-crystal X-ray diffraction data were collected using a STOE imaging-plate diffraction system (IPDS-2T) with graphite-monochromatized Mo Kα radiation. An analytical absorption correction was applied. Direct methods and full-matrix least squares refinements against F² were performed with the SHELXTL package. Crystal data for K₃Ta₂AsS₁₁(**Ia**): monoclinic Cc, Z = 4, a = 14.2571(7) Å, b = 12.4154(7) Å, c = 9.4505(5) Å, β = 100.120(4)°, V = 1646.78(15) Å³ at 100 K, θ_{max} (Mo Kα) = 29.16°, total reflections = 7683, unique reflections F_o² > 2σ (F_o²) = 4151, number of variables = 155, μ = 17.397 mm⁻¹, D_c = 3.657 g cm⁻³, R_{int} = 4.38%, GOF = 1.034, R₁ = 2.15%, R_w = 2.23 for I > 2σ(I). Crystal data for Rb₃Ta₂AsS₁₁(**Ib**): monoclinic Cc, Z = 4, a = 14.4397(8) Å, b = 12.8013(9) Å, c = 9.5687(5) Å, β = 99.289(4)°, V = 1745.55(18) Å³ at 100 K, θ_{max} (Mo Kα) = 29.22°, total reflections = 8079, unique reflections F_o² > 2σ (F_o²) = 4136, number of variables = 155, μ = 24.009 mm⁻¹, D_c = 3.980 g cm⁻³, R_{int} = 4.80%, GOF = 1.047, R₁ = 3.10%, R_w = 3.31 for I > 2σ(I). Crystal data for Cs₃Ta₂AsS₁₁(**II**): monoclinic P2₁/n, Z = 4, a = 9.5967(7) Å, b = 13.5926(7) Å, c = 14.7160(10) Å, β = 98.876(6)°, V = 1896.63(21) Å³ at 100 K, θ_{max} (Mo Kα) = 29.14°, total reflections = 14682, unique reflections F_o² > 2σ (F_o²) = 5058, number of variables = 155, μ = 20.122 mm⁻¹, D_c = 4.161 g cm⁻³, R_{int} = 4.96%, GOF = 1.168, R₁ = 4.19%, R_w = 5.59 for I > 2σ(I).
- (16) Do, J.; Kanatzidis, M. G. *J. Alloys Compd.* **2004**, *381*, 41.
- (17) Stoll, P.; Näther, C.; Bensch, W. *Z. Anorg. Allg. Chem.* **2002**, *628*, 2489.
- (18) Gutzmann, A.; Näther, C.; Bensch, W. *Inorg. Chem.* **2004**, *43*, 2998.
- (19) (a) Wu, Y.; Näther, C.; Bensch, W. *Inorg. Chem.* **2006**, *45*, 8835. (b) Selected bond lengths in K₃Ta₂AsS₁₁(**Ia**) (in Å): Ta(1)–S: 2.206(2), 2.445(2), 2.457(2), 2.484(2), 2.529(2), 2.625(2), 2.813(2); Ta(2)–S: 2.210(1), 2.453(2), 2.466(2), 2.469(2), 2.486(2), 2.501(2), 2.746(2); As–S: 2.232(2), 2.239(2), 2.272(2); S–S: 2.077(2), 2.059(2), 2.095(2). See the Supporting Information for **Ib** and **II**.
- (20) (a) Goh, E. Y.; Kim, S. J.; Jung, D. J. *Solid State Chem.* **2002**, *168*, 119. (b) Evain, M.; Brec, R.; Whangbo, M. H. *J. Solid State Chem.* **1987**, *71*, 244.
- (21) RbTaS₃ is isostructural with CsTaS₃; see the Supporting Information for the details of the synthesis and characterization.
- (22) Liao, J. H.; Marking, G. M.; Hsu, K. F.; Matsushita, Y.; Ewbank, M. D.; Borwick, R.; Cunningham, P.; Rosker, M. J.; Kanatzidis, M. G. *J. Am. Chem. Soc.* **2003**, *125*, 9484.
- (23) (a) Kurtz, S. K.; Perry, T. T. *J. Appl. Phys.* **1968**, *39*, 3798. (b) Ok, K. M.; Chi, E. O.; Halasyamani, P. S. *Chem. Soc. Rev.* **2006**, *35*, 710.
- (24) Banerjee, S.; Malliakas, C. D.; Jang, J. I.; Ketterson, J. B.; Kanatzidis, M. G. *J. Am. Chem. Soc.* **2008**, *130*, 12270.
- (25) Baudrier-Raybaut, M.; Haïdar, R. R.; Kupecek, Ph.; Lemasson, Ph.; Roschner, E. *Nature* **2004**, *432*, 374.
- (26) Nikogosyan, D. N. *Nonlinear optical crystals: a complete survey*; Springer-Science: New York, 2005; p 103.

JA807928D